ROLE OF RETINOCORTICAL PROCESSING IN SPATIAL VISION

Annual Report 2

June 1989

By: D.H. Kelly, Staff Scientist
Sensory Sciences Research Laboratory

Prepared for:

United States Air Force
Air Force Office of Scientific Research
Directorate of Life Sciences
Building 410
Bolling Air Force Base
Washington, D.C. 20332-6448

Attn: Dr. John F. Tangney

Contract F49620-87-K-0009

SRI Project 3558

SRI International
333 Ravenswood Avenue
Menlo Park, California 94025-3493
(415) 326-6200
Telex: 334486

UNCLASSIFIED

SECURITY CLASSIFICATION OF THIS PAGE

REPORT DOCUMENTATION PAGE

Form Approved
OMB No. 0704-0188

1a. REPORT SECURITY CLASSIFICATION Unclassified	1b. RESTRICTIVE MARKINGS
2a. SECURITY CLASSIFICATION AUTHORITY	3. DISTRIBUTION / AVAILABILITY OF REPORT Unlimited
2b. DECLASSIFICATION / DOWNGRADING SCHEDULE	
4. PERFORMING ORGANIZATION REPORT NUMBER(S) Annual Report 2 SRI Project	5. MONITORING ORGANIZATION REPORT NUMBER(S) AFOSR-TR- 89-1027
6a. NAME OF PERFORMING ORGANIZATION SRI International 6b. OFFICE SYMBOL (If applicable)	7a. NAME OF MONITORING ORGANIZATION AFOSR/NL
6c. ADDRESS (City, State, and ZIP Code) 333 Ravenswood Avenue Menlo Park, California 94025	7b. ADDRESS (City, State, and ZIP Code) Bldg 410 Bolling AFB DC 20332-6448
8a. NAME OF FUNDING / SPONSORING ORGANIZATION Air Force Office of Scientific Research 8b. OFFICE SYMBOL (If applicable) NL	9. PROCUREMENT INSTRUMENT IDENTIFICATION NUMBER F49620-87-K-0009
8c. ADDRESS (City, State, and ZIP Code) Directorate of Life Sciences Building 410 Bolling AFB, D.C. 20332-6448	10. SOURCE OF FUNDING NUMBERS PROGRAM ELEMENT NO. 61102F; PROJECT NO. 2313; TASK NO A5; WORK UNIT ACCESSION NO.
11. TITLE (Include Security Classification) Role of Retinocortical Processing in Spatial Vision	
12. PERSONAL AUTHOR(S) Kelly, Donald H.	
13a. TYPE OF REPORT Annual 13b. TIME COVERED FROM 880501 TO 890501	14. DATE OF REPORT (Year, Month, Day) 1989 June 15. PAGE COUNT 30
16. SUPPLEMENTARY NOTATION	

17. COSATI CODES		
FIELD	GROUP	SUB-GROUP
6	16	

18. SUBJECT TERMS (Continue on reverse if necessary and identify by block number)

Spatial vision, retinocortical projection, computational model

19. ABSTRACT (Continue on reverse if necessary and identify by block number)

Continuing the work of Year 1 of this project, we have incorporated our inhomogeneous retinal filtering algorithms into a more general model that includes conformal projection of the retinal filtered outputs into cortical input images, suitable for further processing, such as Gabor filtering. Our new cortical images seem to show much less loss of information relative to the retina. We no longer restore some of the dc (zero-frequency) component that is filtered out by the (Laplacian/Gaussian) retinal receptive-field model. We also provide both right- and left-hemisphere images, joined at the fovea for easy comparison with the corresponding retinal image.

Now that the Year 1 software problems have been solved, study of these cortical images is yielding new insights. For ~~example~~, peripheral objects, while remaining otherwise relatively undistorted, will be rotated either clockwise or counterclockwise as far as ±90 deg in cortical coordinates if they lie above or below the horizontal meridian. This is consistent with other cortical image models, but it does not bode well for the possibility of creating a stable frame by any known array-processing operation on cortical outputs. We are now beginning the third major phase of this project: modeling cortical filtering, as by Gabor functions. It is already clear that a simple, linear convolution without further refinements is not a good model for this process. We hope to develop a better one early in Year 3.

20. DISTRIBUTION / AVAILABILITY OF ABSTRACT ☒ UNCLASSIFIED/UNLIMITED ☐ SAME AS RPT. ☐ DTIC USERS	21. ABSTRACT SECURITY CLASSIFICATION Unclassified
22a. NAME OF RESPONSIBLE INDIVIDUAL Dr. John F. Tangney	22b. TELEPHONE (Include Area Code) (202) 767-5021 22c. OFFICE SYMBOL NL

DD Form 1473, JUN 86 Previous editions are obsolete.

SECURITY CLASSIFICATION OF THIS PAGE

CONTENTS

ILLUSTRATIONS

I RESEARCH OBJECTIVES

As in Year 1, our goal has been to develop a computational model that simulates the front-end stages of human spatial vision, including the retina, retinocortical pathways, and primary visual cortex (V1). This computational product is intended to be a functional, working model, which processes the entire stimulus pattern by appropriate algorithms and can depict its representation at each stage in graphic imagery.

To make this task more manageable, we made important but noncritical simplifications. The model was confined to monocular, photopic, achromatic, quasi-stationary vision. Motion was considered only to the extent that normal spatial processing requires minimal eye movements. Binocularity was considered only by constraining V1 to leave room for interleaved right- and left-eye connections.

Important parts of this complex system have been modeled in other studies. Our main goal is to try to make them all fit together. In doing that, we expected to encounter problems that have not shown up before. When this occurs, we undertake to modify available models and possibly to reinterpret the literature on which they are based.

We achieved our goals of simulating the retinocortical projection and integrating it with inhomogeneous retinal filtering during the first two years of the project (from 1 June 1987 to 30 May 1989). Our next goal is to incorporate into our model the spatial-vision aspects of postsynaptic processing in the visual cortex.

II CURRENT STATUS OF WORK

A. KEY PERSONNEL

In November of 1988, Dr. Grahame Smith, who contributed a great deal to the first year of this project, left SRI Menlo Park for Australia, on assignment to the Australian Artificial Intelligence Institute (A^2I^2). Since we had considerable warning of his departure, we could compensate for its effects on the project. His role was expertly taken over by Dr. Yvan Leclerc, also of SRI's Machine Vision Group. John Peters continued Grahame's programming work, and Grahame stayed in touch by electronic mail and facsimile machine, so that continuity was maintained.

Dr. Smith's departure was the occasion for a thorough study, documentation, and rationalization of the existing LISP code, some of which had been written by Smith and some by Peters. The consolidation work by Leclerc and Peters continued into the early months of 1989. It led to several changes: most were minor but some were not.

B. RETINAL FILTERING AND RETINOCORTICAL MAPPING

At the end of Year 1, we had just taken up the question of choosing a cortical mapping function, and Grahame had investigated the log-polar projection described in Annual Report 1. This representation has now been replaced by the Schwartz conformal mapping function (Schwartz, 1980), discussed below. Although it involves more subtle computations, the Schwartz function was chosen as the best approximation to the known physiology (Tootell, Switkes, et al., 1988) that is currently available. The subroutines for implementing it have been a main focus of the second year's software work, as described below.

1. Reverse-Mapping Procedure

There is a basic difficulty with computer simulation of the cortical projection, to which Dr. Smith provided a simple and elegant solution. In areas of high cortical magnification, near the fixation point, one pixel in the retina maps to many pixels in the cortex. It would be clumsy and time-consuming to project this pixel from the retina to the cortex and then try to find the adjacent locations that should be filled with the same value.

A simpler procedure is to start with the cortical image, initially filled with zeros, and reverse-map these uniformly sampled locations in the cortex back to the retina, in order to find the retinal location corresponding to each cortical pixel. Appropriately scaled (receptive-field) filter functions are then constructed (in *retinal* pixels), and centered at each of these cortically defined (nonuniform) sample points. Each filter function is convolved with

the visual scene (sampled in retinal pixels) and these convolutions provide appropriate values for each cortical input pixel. This is the way in which we now create our cortical input images.

A rough version of this reverse-mapping code was written before Grahame left, but it has since gone through many changes, corrections and additions. We are confident that the present cortical-magnification subroutine now correctly represents the Schwartz projection (Schwartz and Merker, 1986). We chose the receptive-field-size variation independently of the cortical-mapping function, because the two functions are not identical physiologically (Rovamo and Virsu, 1979; Tootell, Switkes, et al., 1988; VanDoorn, Koenderink, et al., 1972). The variation of these two functions with eccentricity in our model is illustrated in Figure 1.

2. Details of the Conformal Projection

Our first algorithm for the Schwartz projection had unwittingly scaled the cortical image independently in the X and Y directions, introducing serious errors in the aspect ratio and local magnification. The interpretation of the mapping function, log (z+c), with respect to the right and left cortical hemispheres was not addressed during Year 1. Setting the so-called species constant, c, equal to 1.0 deg, Grahame had obtained single-hemisphere projections of the type shown in Figure 6 of our previous report (not the Schwartz projection), but this gave an incorrect representation of the cortical image near the fovea.

Our present subroutine sets c = 0.3 deg, which makes the shape of the projection approximately that found in primates (Schwartz and Merker, 1986). We now provide a representation of both hemispheres, showing the visual field on both sides of the fixation point. Negative locations (in the right hemispheric representation), corresponding to small, foveal arguments of log (z+c), are handled simply by translating the entire image (to the right), by the distance log c. The subroutine for left-hemisphere calculations is exactly the mirror image of the right one. We usually juxtapose these two images at the fixation point for ease of comparison with the retinal image.

Figure 2 provides a graphic illustration of the results of this procedure, using the conference-room scene from Annual Report 1. Figure 2(a) shows the retinal image with three selected fixation points, and Figure 2(b) shows the two-hemisphere projection corresponding to the upper-left fixation point. Both retinal and cortical filtering have been removed, to illustrate clearly the form of retinocortical projection we are using. Individual retinal pixels are visible in Figure 2(b) near the fovea. Their distribution is controlled by a uniform cortical distribution, as described above.

Figure 2(b) does not occur as a stage in our model, but it can be compared with the conformal projection images made by Schwartz, who did not take retinal or cortical filtering into account (Schwartz and Merker, 1986). He gave no details of the construction of his two-hemisphere images, but their appearance suggests that his right- and left-hemispheric

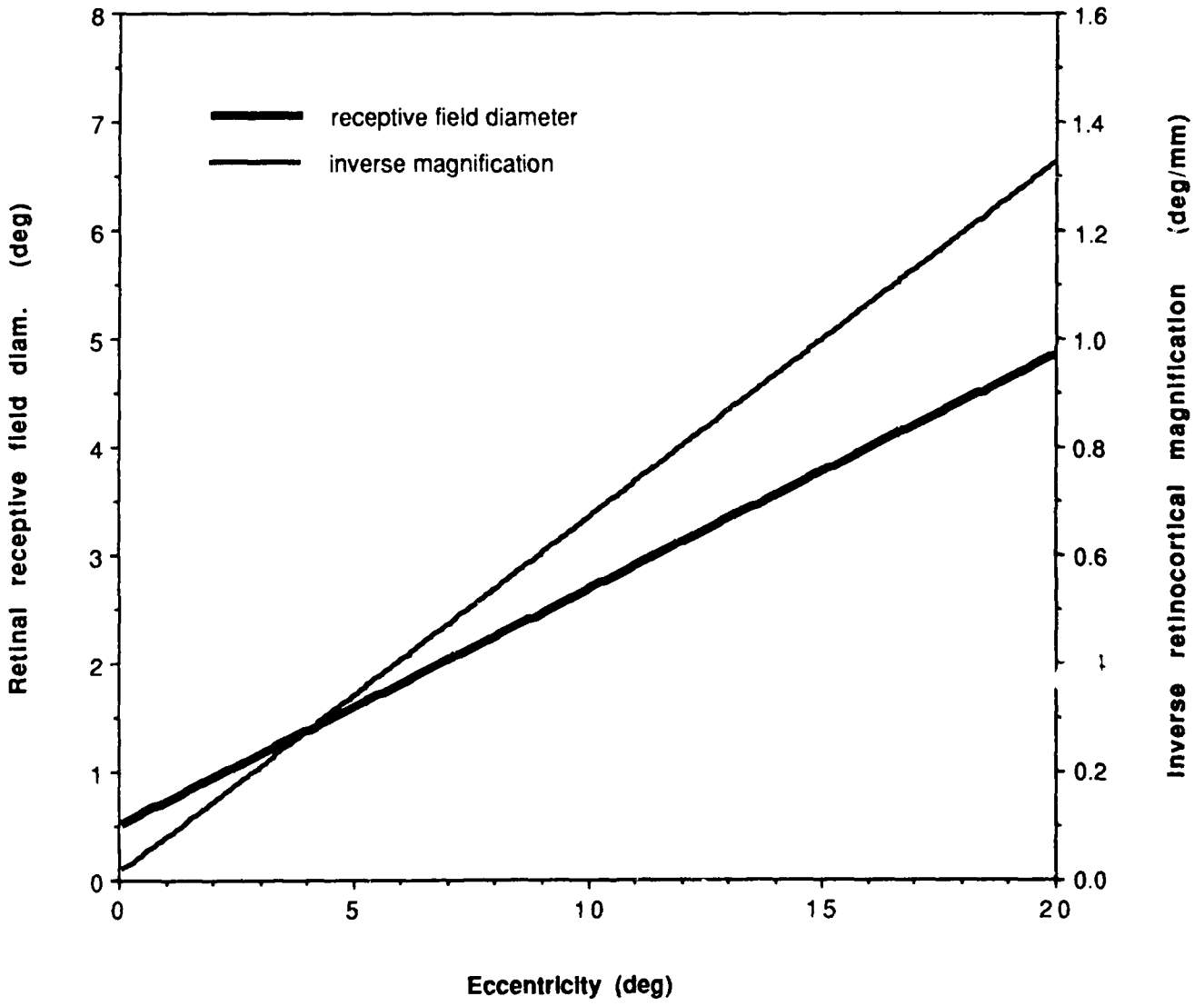

FIGURE 1 COMPARISON OF RETINAL INHOMOGENEITY WITH RETINOCORTICAL PROJECTION, AS FUNCTIONS OF ECCENTRICITY

Heavy line: receptive-field diameter used in our retinal-filtering algorithm, as a function of eccentricity.
Light line: inverse of the retinocortical magnification determined from log (z + 0.3), averaged over all meridians.

(a) CONFERENCE-ROOM SCENE, SHOWING THREE FIXATION POINTS USED FOR SUBSEQUENT PROCESSING

(b) UNFILTERED CORTICAL MAPPING OF SAME SCENE, WITH UPPER-LEFT FIXATION SHOWN IN (a)

FIGURE 2 EXAMPLE OF SCHWARTZ CONFORMAL PROJECTION WITHOUT FILTERING

projections were in fact joined by the translation-reflection procedure just described. We will occasionally include unfiltered projections such as Figure 2(b) in this report, for purposes of comparison.

C. GABOR FILTERING OF CORTICAL IMAGES

With the availability of correctly computed cortical inputs, we can now attempt to simulate an important spatial aspect of cortical processing sometimes known as Gabor filtering. We believe this is the first time that has been done with retinally filtered, conformally mapped cortical images.

Two-dimensional Gabor functions, which are one-directional sine waves with two-dimensional Gaussian envelopes, have previously been used to model cortical receptive fields (Daugman, 1985), as have other, Gabor-like functions (such as Gaussian derivatives or differences of gaussians). Available data are probably insufficient to choose any of these alternatives on the basis of goodness of fit. We chose Gabor functions here in the same way that we chose our retinal filter functions; the chosen functions are well known and simple to compute.

1. Details of the Gabor Computations

This was the first part of our simulation where we could assume at least approximate homogeneity, so we took advantage of the convolution theorem. Instead of convolving a given Gabor filter with the cortical input, we took the (two-dimensional) Fourier transform of both, multiplied these frequency functions together, and inverse-transformed the product to obtain the desired result. Figure 3(a) shows the frequency spectrum of a vertically oriented Gabor function, and Figure 3(b) shows its inverse transform. These are even-symmetric functions. Odd-symmetric Gabor functions would also be required for image coding (Daugman, 1987), but such Hilbert pairs will not be treated further in this report.

Although much simpler to implement, this convolution algorithm involved a few unexpected problems. To center the spectrum of the Gabor filter, it was necessary to know the coordinates of the origin of the fast Fourier transform (FFT) subroutine in ImagCalc™. As this FFT had been used mainly to obtain power spectra (amplitudes but no phase information), its origin was undocumented; however, it turned out to be in the lower left corner.

Another peculiarity of the FFT involved scaling. If the number of pixels across the image is less than 2^n (where n = any integer), any FFT will fill the remainder with zeros before transforming it. In the two-dimensional case, as long as the image is square, the square spectrum does not result in scaling problems. But if the image is not square (as ours are not) ImagCalc™ still keeps its spectrum square; thus its horizontal and vertical scale factors may differ by a power of 2. Since the inverse transform undoes this distortion, it has no effect in some applications. However, since our Gabor functions were created as Gaussian blobs in the frequency domain, they had to be distorted beforehand in

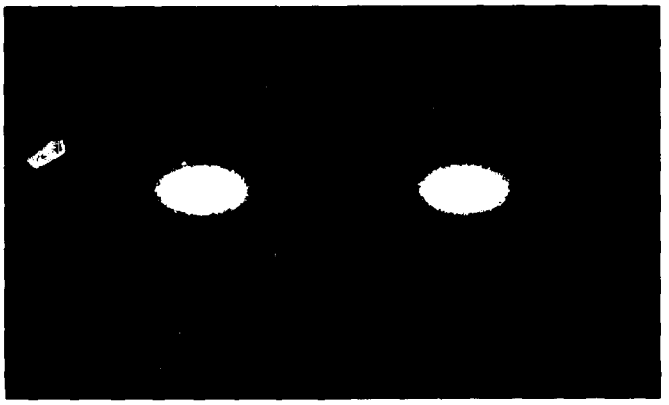

(a) FREQUENCY SPECTRUM OF VERTICAL GABOR FUNCTION USED IN CORTICAL SIMULATION

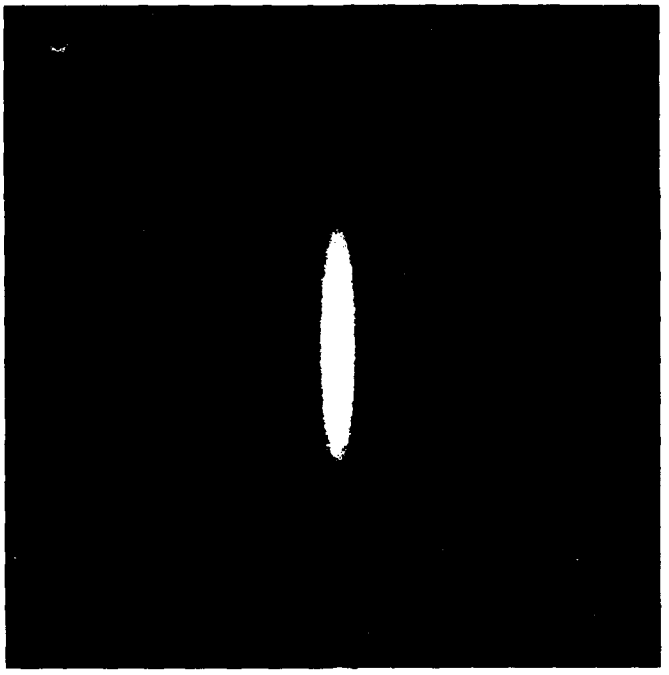

(b) INVERSE, TWO-DIMENSIONAL FOURIER TRANSFORM OF (a)

FIGURE 3 STANDARD FORM OF EVEN GABOR FILTER

order to inverse-transform correctly. We used Gabor functions with the standard shape of Daugman's "polar wavelet" family (Daugman,1988), with frequency bandwidth twice the orientation bandwidth (30 deg)

2. Interaction Between Retinal and Cortical Filtering

The frequencies and orientations of the first Gabor filters we used were chosen to avoid a fundamental theoretical problem: Post-synaptic cortical potentials that show Gabor-like receptive fields are not measured relative to any retinally filtered cortical input, but rather with respect to the distal stimulus pattern, which is the definition of a receptive field (Daugman 1985). Thus, cortical receptive fields necessarily represent the effects of consecutive retinal, LGN, and cortical filtering. Therefore, even neglecting LGN effects (as our model does), it would be necessary in principle to deconvolve the (Laplacian/ Gaussian) retinal filtering from the Gabor-like end result, in order to see the "true" cortical filter.

This retinocortical interaction is not very apparent, however, partly because the bandwidths of the retinal filters are considerably greater than those of the cortical filters (Kelly and Burbeck 1984). Thus, if we carefully center our Gabor filters within the passband of the (remapped) retinal filters, their interaction should be minimal. (In the limit, i.e., for an all-pass retina, deconvolution would have no effect.) We located the retinal passband of our model experimentally, by transforming cortical input images to the frequency domain, and chose our Gabor filters accordingly. The resulting Gabor functions are the ones used for the Gabor-filtering results reported here.

The efficacy of this procedure could be tested by substituting an all-pass (identity) filter for our retinal filters and then determining whether this changes the Gabor-filtered cortical output significantly. We plan to make such tests during the next project period.

D. GRAPHIC RESULTS

In this section we provide representative illustrations of the information contained at various stages of our retinocortical model. Because images like these have not been created before, it seemed worthwhile to provide several examples for each stage. If it is true that "a picture is worth 10,000 words," they should contribute greatly to the brevity of this report.

1. Retinal-Filtered Cortical Inputs

Although our retinal-filtering subroutines were substantially complete in the first year of this project, they had not been married to the cortical-projection technique described above. Thus the construction of retinal-filtered, cortical "input images," correct in detail to the best of our knowledge, was an important achievement of Year 2, which we illustrate here with examples of these images, and illustrations of how they are affected by changes of fixation.

Figure 4 shows the retinal-filtered, cortical input corresponding to Figure 2(a) and (b). Although there is no dc (zero-frequency component) in this image (large areas are all the same shade of gray) and edges are rather coarsely represented, surprisingly little information about the scene is destroyed by retinal filtering. The same is true of all the other cortical inputs illustrated in this section.

Figures 4 and 6-16 also illustrate that retinocortical magnification in our model compensates for retinal inhomogeneity reasonably well, except in the vicinity of the fovea, where it overcompensates (more magnification). This extra magnification is shown quantitatively in Figure 5, obtained by taking the ratio of the two curves plotted in Figure 1. The cortical distance calculated in this way is fairly constant for eccentricities greater than a few degrees, but increases rapidly near the fovea. This seems to be a realistic representation of the physiological data we used for the model.

Figure 6 shows the projected, filtered and unfiltered images corresponding to the lower fixation point in Figure 2(a). Comparing this fixation with the one shown in Figures 2(b) and 4, we can see that objects far from the fixation point, although relatively undistorted, are rotated when the fixation point is elevated or depressed. (Note the person on the right side of the visual field.)

Figure 7 shows the projected, filtered image corresponding to the upper-right fixation point in Figure 2(a). Here the person on the left has been rotated almost 90 degrees, relative to his position in Figure 6. When a human subject raises or lowers his direction of gaze, he does not perceive any such rotation of peripheral objects, of course. But this graphically illustrates one of the problems involved in assembling information from multiple fixations after they have been processed by V1. Does Gabor filtering, or some other known physiological mechanism, facilitate the assembly process? That is the chief remaining question to be pursued in this project.

The peripheral-rotation effect could be quantified by aiming our model at a rectilinear grid or checkerboard target. But the main entrance of SRI, shown in Figure 8, serves equally well. Here the fixation point is near the center of a two-story facade, with vertical columns and rectangular windows. Lines near the horizontal meridian remain horizontal in the cortical image, all the way to the edges of the 40-deg visual field shown here. But vertical lines project to parabolic arcs, steepest near the vertical meridian but not straight anywhere.

We conclude this section with similar treatments of two portraits, familiar if not standard in the image-coding and computer vision community. Figure 9 shows the "Lena" picture, with three different fixation points marked as in Figure 2(a). Figures 10, 11, and 12 illustrate cortical inputs for the center, upper right, and left fixations, respectively. The features just described—extra magnification near the fovea and object rotation in the

FIGURE 4 RETINALLY FILTERED, CORTICALLY MAPPED VERSION OF CONFERENCE-ROOM SCENE, WITH UPPER-LEFT FIXATION AS IN FIGURE 2(b)

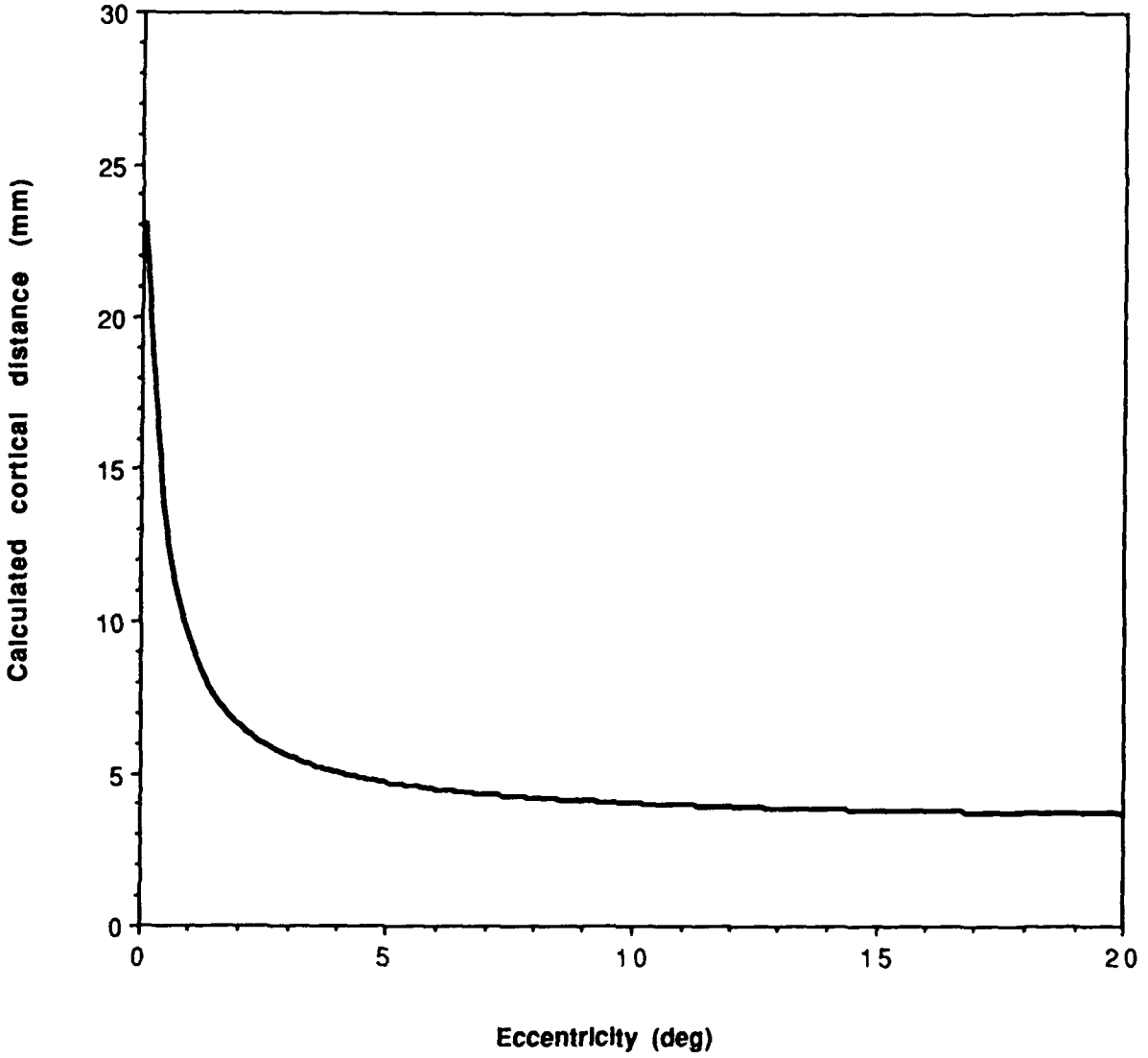

FIGURE 5 RATIO OF THE TWO CURVES IN FIGURE 1

If cortical magnification exactly compensated for retinal inhomogeneity, this ratio would be constant.

(a) UNFILTERED CORTICAL MAPPING

(b) RETINALLY FILTERED VERSION OF (a)

FIGURE 6 CONFERENCE-ROOM SCENE, WITH LOWER FIXATION POINT SHOWN IN FIGURE 2(a)

FIGURE 7 RETINALLY FILTERED, CORTICALLY MAPPED VERSION OF CONFERENCE-ROOM SCENE, WITH UPPER-RIGHT FIXATION POINT SHOWN IN FIGURE 2(a)

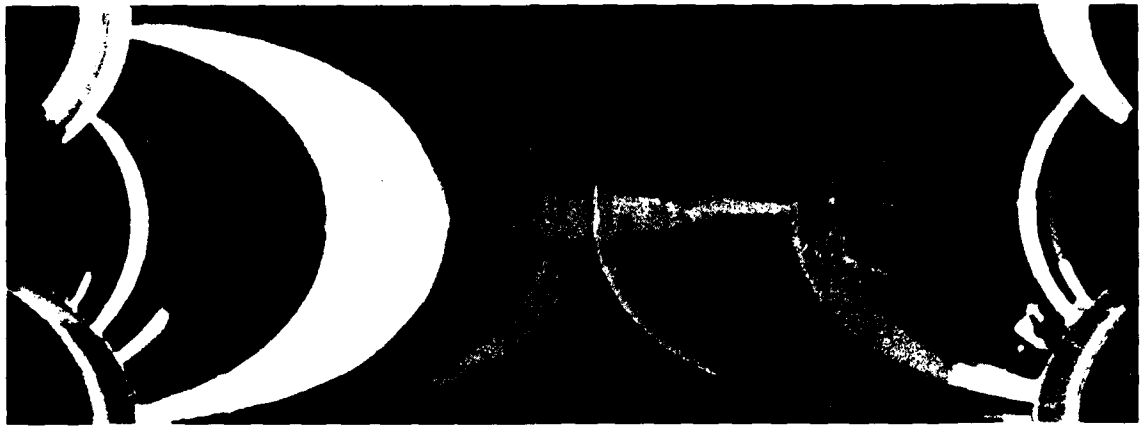

(a) UNFILTERED CORTICAL MAPPING

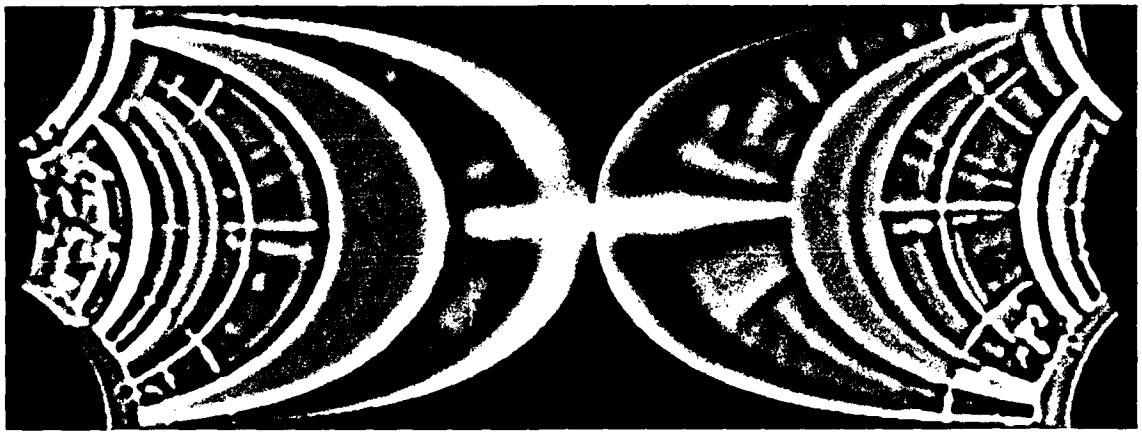

(b) RETINALLY FILTERED VERSION OF (a)

FIGURE 8 BUILDING FACADE SCENE, WITH FIXATION BETWEEN COLUMNS

FIGURE 9 LENA PORTRAIT, SHOWING THREE FIXATION POINTS USED FOR SUBSEQUENT PROCESSING

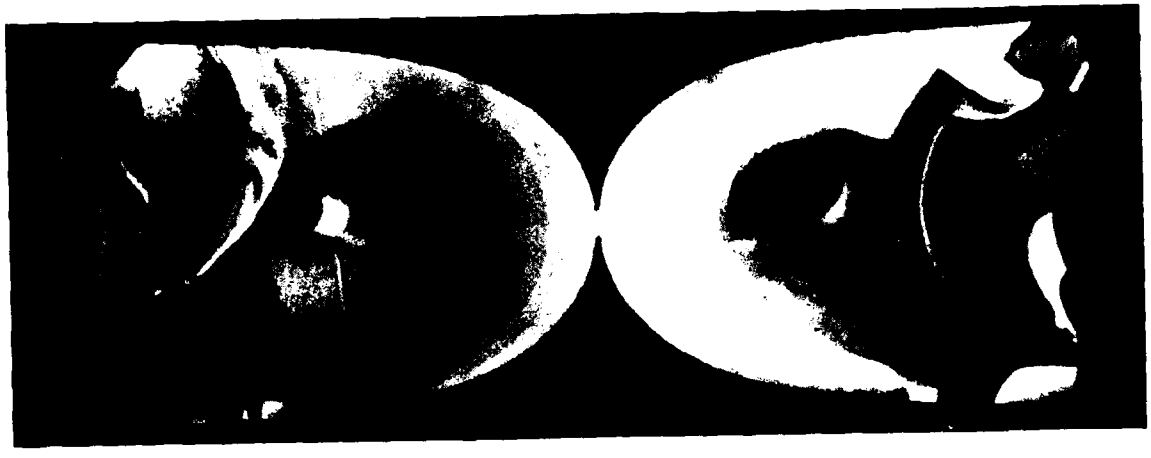

(a) UNFILTERED CORTICAL MAPPING

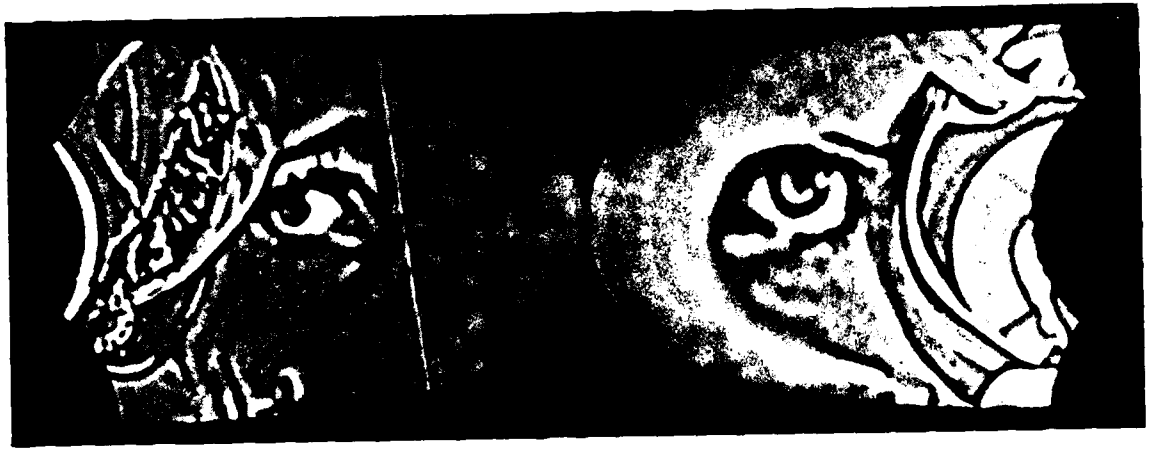

(b) RETINALLY FILTERED VERSION OF (a)

FIGURE 10 LENA PORTRAIT, WITH CENTER FIXATION POINT SHOWN IN FIGURE 9

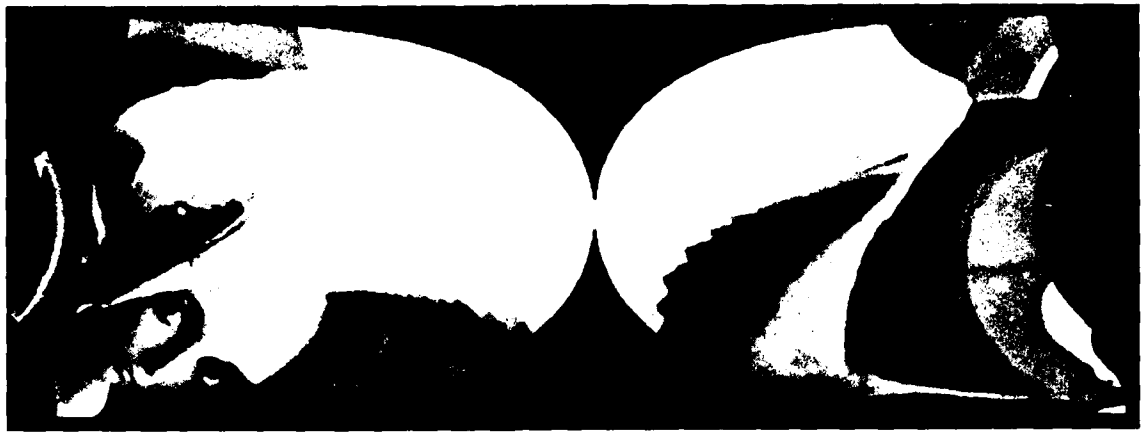

(a) UNFILTERED CORTICAL MAPPING

(b) RETINALLY FILTERED VERSION OF (a)

FIGURE 11 LENA PORTRAIT, WITH UPPER-RIGHT FIXATION POINT SHOWN IN FIGURE 9

(a) UNFILTERED CORTICAL MAPPING

(b) RETINALLY FILTERED VERSION OF (a)

FIGURE 12 LENA PORTRAIT, WITH LOWER-LEFT FIXATION POINT SHOWN IN FIGURE 9

periphery—are readily apparent.Finally, Figures 13-16 show similar treatments of the full-face mandrill picture, again with three fixation points. These four scenes constitute our entire library, but with our ability to select arbitrary fixation points, they seem to be more than sufficient for our plans in the foreseeable future.

2. Gabor-Filtered Cortical Outputs

In image-coding studies, the purpose of Gabor filtering is simply to reproduce the original image by way of a code that uses many fewer bits/pixel, and this can be done quite successfully (Daugman, 1988). In our case, however, the application is quite different and presents its own unique problems. Gabor filtering was incorporated in our model because something similar is known to be performed in the visual cortex, V1 (Daugman, 1980; Jones and Palmer, 1987). Its relation to retinal inhomogeneity and cortical magnification is considered here for the first time, as far as we know. Moreover, in order to try to understand how the cortical outputs from various fixations are assembled, it seems essential to include some form of Gabor filtering.

Up to this point we have been able to display the results of each stage of visual processing graphically, as a single, two-dimensional array of signal strengths, or an *image*. This was possible only because of the simplifying assumptions introduced at the start of this project. At this point, however, we seem to need another such assumption (or assumptions).

The output of a general, Gabor-filtering process is not one image but several (Daugman, 1988), each corresponding to a Gabor function of a particular frequency, symmetry, and orientation, like the components of a cortical hypercolumn. How shall we choose one of these images? Or if they are to be combined in some way, how shall we combine them? As usual, we started with the simplest useful operation we could perform.

Our Gabor-filtered results, like the other illustrations, are shown on a black background for clarity. However, we inserted the background only after the final transform step (see Subsection C.1). During the FFT computations, we used a gray background equal to the average value of the image, to eliminate any dc component. Figure 17(a) shows the result of filtering the cortical input of Figure 4 with the vertical Gabor function shown in Figure 3(b). In Figure 17(b), the same image has been filtered with a horizontal Gabor function of the same frequency. In Figure 18, the same two filters have been applied to the image of Figure 6(b), which is another fixation of the same scene.

Orientation selectivity is the most important property of Gabor filters, but extracting a single orientation in this way does not convey much information about the scene, even with a Gabor function tuned to the retinal prefiltering (see Subsection C.2). The most prominent horizontal and vertical features in any one fixation seem unrelated. More significant for our purposes, the most prominent features in one fixation seem unrelated to those in the other, for either orientation. Similar results for vertical and horizontal filtering at various fixations were obtained with the two portraits, but these are not shown here.

FIGURE 13 MANDRILL FACE, SHOWING THREE FIXATION POINTS USED FOR SUBSEQUENT PROCESSING

(a) UNFILTERED CORTICAL MAPPING

(b) RETINALLY FILTERED VERSION OF (a)

FIGURE 14 MANDRILL FACE, WITH CENTER FIXATION POINT SHOWN IN FIGURE 13

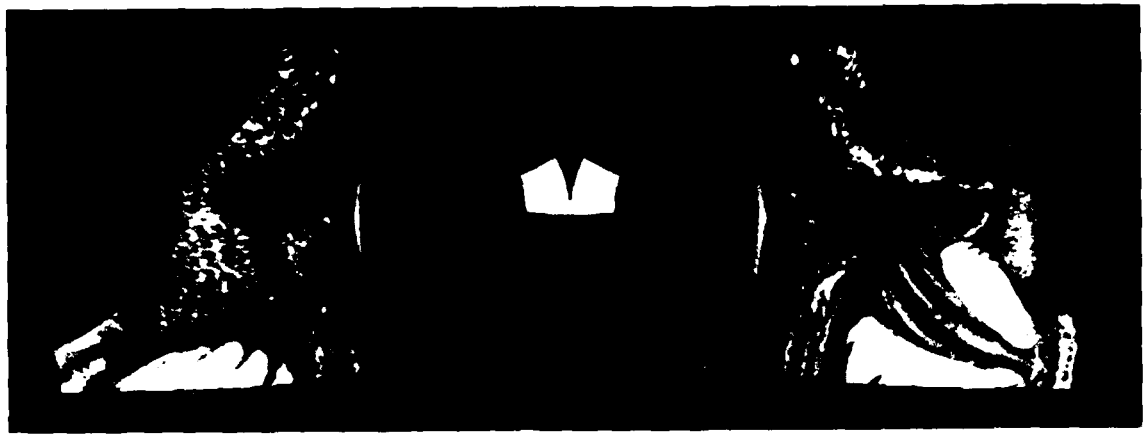

(a) UNFILTERED CORTICAL MAPPING

(b) RETINALLY FILTERED VERSION OF (a)

FIGURE 15 MANDRILL FACE, WITH FIXATION POINT AT LEFT EYE AS SHOWN IN FIGURE 13

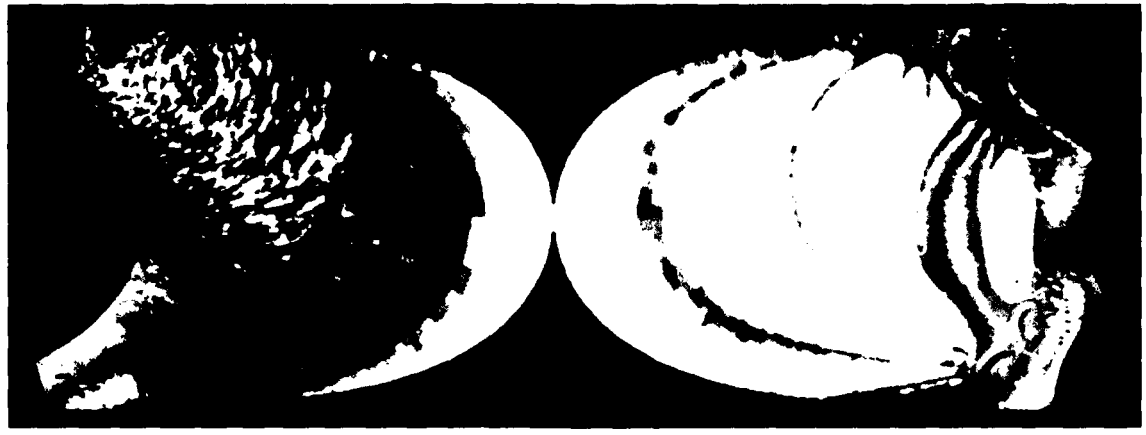

(a) UNFILTERED CORTICAL MAPPING

(b) RETINALLY FILTERED VERSION OF (a)

FIGURE 16 MANDRILL FACE, WITH LEFT-CENTER FIXATION POINT SHOWN IN FIGURE 13

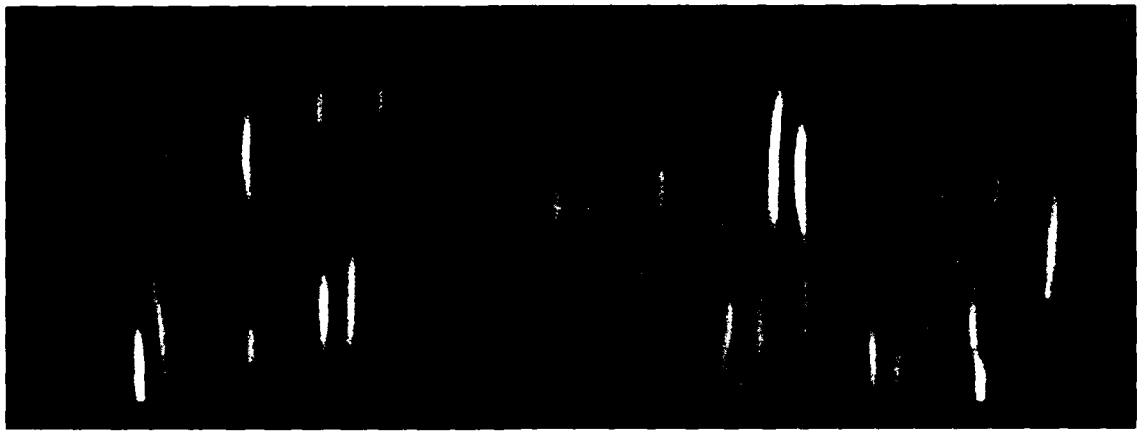

(a) WITH VERTICAL GABOR KERNEL SHOWN IN FIGURE 3(b)

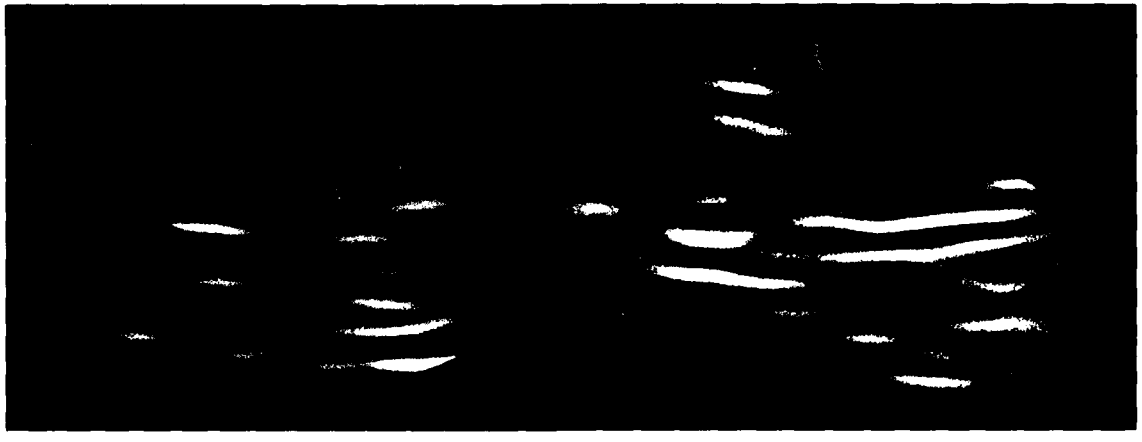

(b) SAME AS (a) BUT WITH HORIZONTAL KERNEL

FIGURE 17 LINEAR FILTERING OF CORTICAL INPUT SHOWN IN FIGURE 4 (conference room, upper-left fixation)

(a) WITH VERTICAL GABOR KERNEL SHOWN IN FIGURE 3(b)

(b) SAME AS (a) BUT WITH HORIZONTAL KERNEL

FIGURE 18 LINEAR FILTERING OF CORTICAL INPUT SHOWN IN FIGURE 6(b) (conference room, lower fixation point)

One important reason for this lack of correlation is the peripheral-rotation effect discussed in Subsection D.1 and mostly clearly illustrated in Figure 8. Figure 19 shows the same vertical and horizontal Gabor filters applied to Figure 8(b). Note that the columns of the facade, although vertical in the original scene, shift from the vertical-feature image to the horizontal one with increasing eccentricity. The effect is particularly evident in the left hemisphere for this fixation.

These results are not really surprising because this type of homogeneous, linear operation is not a very good model for the known physiology. There is no reason to expect any specialized cooperation among just those cells from every orientation column that happen to have the same orientation in cortical coordinates. A less arbitrary hypothesis might involve cooperation among oriented units that follow the external coordinate system suggested by Figure 8. That is still too constraining, however, since it implies a world made of horizontal and vertical lines. What we need is a Gabor filtering process that responds to the input orientations in an adaptive, nonlinear way.

Taking a leaf from the image-coding studies (Daugman, 1987), however, we might hope that such a process could be constructed from linear, homogeneous building blocks, like those just described. This will be our first approach in the coming year.

E. SUMMARY AND FUTURE PLANS

In Year 1, we were mainly concerned with inhomogeneous filtering in the retina; in Year 2, we worked with retinocortical projection and its integration with retinal inhomogeneity. Having successfully completed the software for simulating and displaying the results of these two operations, we are now prepared to start the third (and most difficult) phase of this project: implementation of the postsynaptic cortical mechanisms of spatial vision (perhaps, post-V1). We will start, as usual, by building on the results achieved thus far, following some of the suggestions given above.

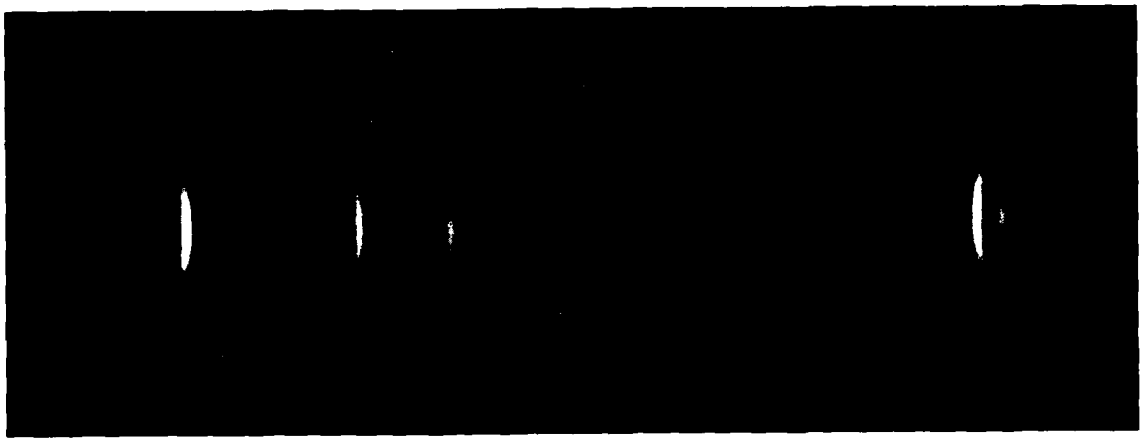

(a) WITH VERTICAL GABOR KERNEL SHOWN IN FIGURE 3(b)

(b) SAME AS (a) BUT WITH HORIZONTAL KERNEL

FIGURE 19 LINEAR FILTERING OF CORTICAL INPUT SHOWN IN FIGURE 8(b) (building facade)

III RESEARCH PERSONNEL

D. H. Kelly, Principal Investigator (Visual Sciences Program)

John D. Peters, Research Assistant (Visual Sciences Program)

Yvan G. Leclerc, Computer Scientist (Artificial Intelligence Center)

REFERENCES

Daugman, J.G., 1980: "Two-dimensional spectral analysis of cortical receptive field profiles," *Vision Res.*, Vol. 20, pages 847-856.

Daugman, J.G., 1985: "Uncertainty relation for resolution in space, spatial frequency, and orientation optimized by two-dimensional visual cortical filters," *J. Opt. Soc. Am. A.*, Vol. 2, pages 1160-1169.

Daugman, J.G., 1987: "Image analysis and compact coding by oriented 2D Gabor primitives," *SPIE Proceedings*, Vol. 758 (April).

Daugman, J.G., 1988: "Complete discrete 2-D Gabor transforms by neural networks for image analysis and compression," *IEEE Trans. ASSP*, Vol. 36, pages 1169-1179.

Jones, J., and L. Palmer, 1987: "An evaluation of the two-dimensional Gabor filter model of simple receptive fields in cat striate cortex," *J. Neurophysiol.*, Vol. 58, pages 1233-1258.

Kelly, D.H., and C.A. Burbeck, 1984: "Critical problems in spatial vision," *CRC Cr. Rev. Biomed. Engng.*, Vol. 10, pages 125-177.

Rovamo, J., and V. Virsu, 1979: "An estimation and application of the human cortical magnification factor, " *Exp. Brain Res.*, Vol. 37, pages 495-510.

Schwartz, E.L., 1980: "Computational anatomy and functional architecture of striate cortex," *Vision Res.*, Vol. 20, pages 645-669.

Schwartz, E.L., and B. Merker, 1986: "Computer-aided neuroanatomy: Differential geometry of cortical surfaces and an optimal flattening algorithm," *IEEE Trans. CG&A*, Vol. 6, pages 36-44.

Tootell, R.B.H., E. Switkes, M.S. Silverman, and S.L. Hamilton, 1988: "Functional anatomy of macaque striate cortex. II. Retinotopic organization," *J. Neuroscience*, Vol. 8, pages 1531-1568.

VanDoorn, A.J., J.J. Koenderink, and M.A. Bouman, 1972: "The influence of retinal inhomogeneity on the perception of spatial patterns," *Kybernetik* , Vol. 10, pages 223-230.

Appendix

CODE STATISTICS

All code was written in Symbolics Common LISP and run on a Symbolics 3600-series LISP machine. This code also made extensive use of the ImagCalc™* vision system.

Cortical transformation code:

Total lines of code	853 lines
Run time for unfiltered cortical projection	2 minutes; 7 seconds
Run time for filtered cortical projection	5 hours, 8 minutes
Average retinal-filter convolution run time	0.0996 second

Gabor filtering code:

Total lines of code (not including ImagCalc FFT)	182 lines
Run time for Gabor convolution	15 minutes, 50 seconds

Run times for the cortical transformation were measured while running with a 40-degree field on a 650- by 496-pixel retinal input image, producing a 743- by 248-pixel cortical output image. The Gabor convolution run time was measured while processing a 743- by 248-pixel cortical image.

*ImagCalc™ is a trademark of SRI International.